Journal of Testing and Evaluation, Vol. 34, No. 6
Paper ID JTE100030
Available online at: www.astm.org

Thomas J. Urbanik,[1] *Sung K. Lee,*[2] *and Charles G. Johnson*[3]

Column Compression Strength of Tubular Packaging Forms Made from Paper

ABSTRACT: Tubular packaging forms fabricated and shaped from rolled paper are used as reinforcing corner posts for major appliances packaged in corrugated containers. Tests of column compression strength simulate the expected performance loads from appliances stacked in warehouses. Column strength depends on tube geometry, paper properties, basis weight, and number of laminations. A column strength model considers the tube geometry to be a sequence of geometric flat and arched segments with each segment apt to fail by either buckling or compression. Contributions of segments to strength depend on respective failure modes and are appropriately summed. The principles of our derived model provide insight into the optimum paper properties and number of laminations in the selection and design of tubular posts.

KEYWORDS: corner post, compression strength, insert, column buckling

Introduction

The shipment of major household appliances, such as washing machines, kitchen ranges, and refrigerators, was reported by the Department of Commerce to be valued at $18 billion in 2003 [1]. Shipment and storage activity includes a period during which the appliances, packaged in corrugated containers, are stacked in warehouses and moved around by clamp trucks. The corrugated container ideally functions as a wrapper around a set of protective corner posts that are added to increase container stacking strength and to cushion the appliance from lateral compression during clamp truck handling.

The type of corner posts examined in this study is the tubular packaging form manufactured by Sonoco Products Company (Hartsville, South Carolina). These tubular packaging forms are fabricated by rolling and gluing paper around a cylinder, then reforming the round tube in a mandrel conforming to the edge geometry of the appliance. A length of paper is cut from its roll and fed sideways to be rolled and glued. The machine direction (MD) of the paper becomes aligned with the axis direction of the post. Figure 1 shows various cross-sectional shapes of tubular packaging.

Column compression strength, lateral cushioning stiffness, and beam bending stiffness are all important performance characteristics of the corner post. Column compression strength is a function of paper furnish and basis weight, number of paper laminations, and load sharing among geometrically flat and arched segments comprising its geometry. The MD properties of the paper are of most interest in understanding column strength, but the cross machine direction (CD) properties also play a role.

The Forest Products Laboratory and Sonoco Products Company collaborated in a study of tubular packaging forms to determine an engineering-driven methodology of design. The objective was performance prediction software to assist the tube manufacturing engineer and the appliance product engineer in rapidly examining packaging and product alternatives. Success would enable the tube manufacturer to minimize paper costs and fabrication hardware, and would enable the appliance manufacturer to eliminate appliance framework that functions only to resist warehouse-induced stresses.

The scope of this study examines the performance criterion of

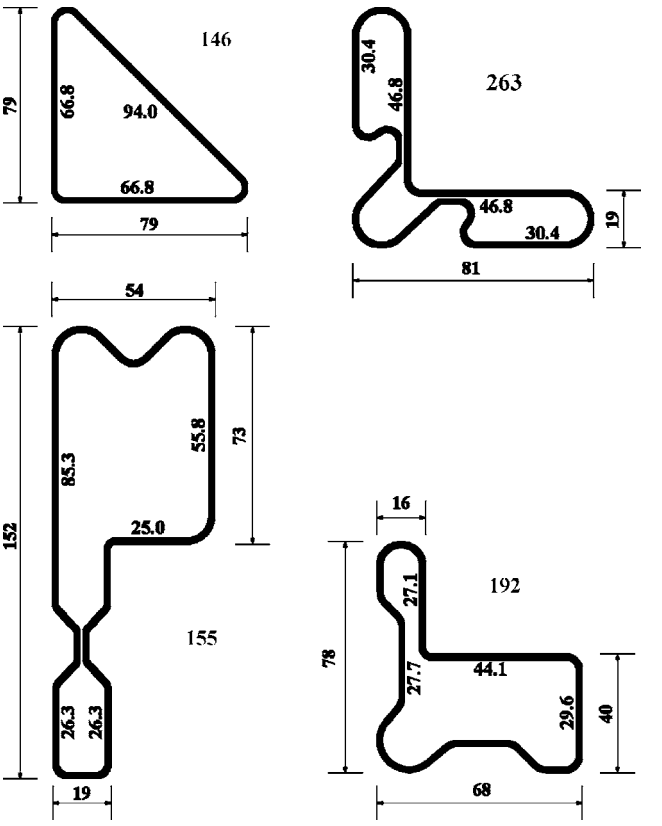

FIG. 1—*Cross-sectional geometry of tubular packaging forms 146, 155, 192, and 263 used in study. Dimensions shown are in millimeters. Numbers within figures are width dimensions of flat plate segments apt to buckle.*

Manuscript received November 21, 2005; accepted for publication March 31, 2006; published online May 2006.

[1]Research Engineer, Forest Products Laboratory, One Gifford Pinchot Drive, Madison, WI 53705.

[2]Formerly with Forest Products Laboratory; currently Director of Global Logistics & Indirect Strategic Sourcing, Welch Allyn, Inc., Skaneateles Falls, NY.

[3]Formerly with Sonoco Products Company, Hartsville, SC.

TABLE 1—*Column compression strength of tubular packaging forms in relation to experimental design*[a]

Tube style	BW g/m^2	Lam. (N)	Tube Perimeter (p) mm	Buckling Prone Segment Width (l)[b] mm				Crush-Prone Width (l_c)[c] mm	Strength (P) Experimental Avg. kN	Experimental CV %	Predicted kN	Difference %
146	205	6	261	94.0	*66.8*	…	…	33.6	2.72	5.97	2.48	−8.88
	244	4	261	94.0	*66.8*	…	…	33.6	2.09	4.72	2.05	−1.62
	244	5	261	94.0	*66.8*	…	…	33.6	3.19	7.46	3.25	1.68
	244	6	261	94.0	*66.8*	…	…	33.6	5.09	6.11	5.16	1.44
	342	4	261	94.0	*66.8*	…	…	33.6	4.09	2.46	3.46	−15.4
155	205	4	401	85.3	55.8	*26.3*	25.0	182	3.31	4.46	3.77	14.0
	244	3	401	85.3	55.8	*26.3*	25.0	182	3.92	2.98	4.10	4.62
	244	4	401	85.3	55.8	*26.3*	…	207	6.02	3.10	6.63	10.2
	342	3	401	85.3	55.8	…	…	260	5.77	5.14	4.42	−23.4
192	205	5	300	44.1	…	…	…	255	3.95	2.52	3.81	−3.47
	244	3	300	44.1	29.6	27.7	27.1	171	2.78	5.68	3.79	36.4
	244	5	300	44.1	…			255	7.09	2.34	7.30	3.05
	342	3	300	44.1	29.6	27.7	…	198	4.52	3.30	5.63	24.4
263	205	4	330	*46.8*	*30.4*	…	…	176	3.00	5.84	3.12	3.97
	205	5	330	*46.8*	…	…	…	236	4.27	3.28	4.01	−6.13
	342	3	330	*46.8*	*30.4*	…	…	176	5.63	4.83	5.57	−0.94
	342	5	330	*46.8*	…	…	…	236	12.6	3.69	11.86	−5.66

[a]BW is nominal basis weight of paper; Lam, laminations; CV, coefficient of variation.
[b]Segments with l dimension in italics are counted twice.
[c]Cumulative width.

column compression strength emanating from the collaboration. Buckling theory developed by Johnson and Urbanik [2] and successful with corrugated fiberboard microplates was applied to the packaging form segments. A model is developed that relates column compression strength to the summation of segment strengths as characterized by buckling or crushing failure. In actual service the corner posts are sandwiched between the corners of the box and the edges of the appliance. Compression loads are transmitted to the posts through the box flaps. The combined loading condition and boundary conditions in actual service could be difficult to model. The analysis of this study is limited to the column compression of posts in a laboratory compression machine.

Experimental Design

Four tubular packaging form geometries (forms 146, 155, 192, and 263 (Fig. 1)) with features providing a broad test of theory were selected for fabrication from over 200 candidates. Tubes were fabricated with three to six laminations of one of three nominal basis weight (BW) grades of paper: 205, 244, or 342 g/m^2. Tubes were fabricated into 17 combinations, with the number of laminations depending on tube style (Table 1). Tubes were numbered sequentially during production, and paper stock was intermittently sampled for later experimental characterization and correlation with tube performance.

All tests of paper, laminates, and tubes were conducted in a conditioned environment at 23°C and 50 % relative humidity (RH) in accordance with ASTM Standard D 685-93 [3] after preconditioning the materials in a dry environment below 30 % RH followed by conditioning the materials at 50 % RH. Compression specimens of paper, laminates, and tubes were cut to a specific length and loaded at a corresponding rate so as to yield the same material strain rate among all specimen types.

Material Characterization

Among the numerous test methods for determining paper compression strength and extensional stiffness, Gunderson [4] developed a vacuum compression apparatus (VCA) that yields the continuous compression load-deformation response of a 27 × 95 mm paper strip. The VCA load-deformation curves were produced for MD and CD specimens sampled along the continuous paper stock. Data on stress σ varying with strain ε were reduced to average parameter values c_1 and c_2 in a fit of the equation

$$\sigma = c_1 \tanh(c_2/c_1\varepsilon) \quad (1)$$

up to the maximum stress σ_u. The curve fitting procedure is described by Urbanik [5]. Stress was determined from load per unit area based on the surface-to-surface thickness h according to Tappi T 411 [6].

Typical load-strain data for a one-ply curve and the four-ply curve predicted by 4 hc_1 and 4 hc_2 are shown in Fig. 2. Data averages from ten specimens of each combination of material and loading direction are summarized in Table 2. For comparison with VCA data, data on σ_u determined by the ring crush method following Tappi T 818 [7] are also given. In contrast with the ring crush apparatus, the VCA is designed to support the paper specimen against lateral buckling up to its intrinsic edgewise crush strength. Significant differences between VCA and ring crush maximum stress were observed, particularly in the machine direction (Table 2).

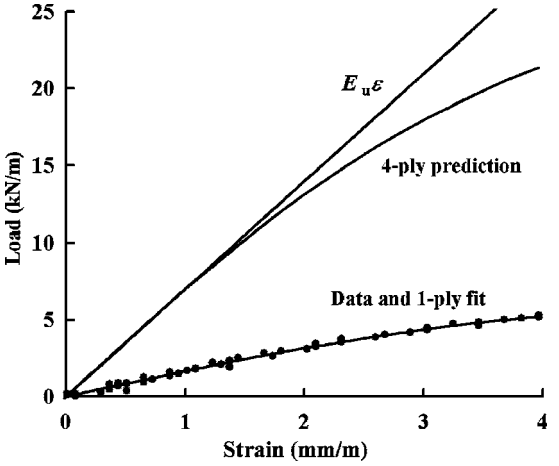

FIG. 2—*Representative compression load-strain data of 205 g/m² paper in MD scaled in proportion to average fitted load-strain curve. Predicted four-ply compression curve is compared with initial slope of average load-elongation curve obtained from tension tests of corresponding four-ply laminates.*

Table 2 also shows values for the ratio of CD c_2 relative to MD c_2. The CD/MD ratio is used to express the transverse properties of a paper lamination relative to the axial properties in the loading direction.

Extension tests were also performed on laminated specimens cut from the packaging forms for comparison with paper tests. The laminate thickness exceeded the compression testing ability of the VCA, and screw-driven tension tests were substituted. Smooth-edged 13 × 76 mm specimens were prepared by a laser cutting device by Corporate Custom Products, Inc. (Madison, WI). Specimen length was chosen as the largest practical size among the flat sections of packaging form geometry that would yield a tension strain rate equal to the compression strain rate of the paper test specimens. Average initial extensional stiffness (E_u) values from ten specimens of each combination of BW, number of laminates (N), and loading direction are compared with VCA predictions in Table 3.

An example of an average initial slope of a four-ply load-elongation curve is compared with the predicted compression curve in Fig. 2. If the effects of adhesive and specimen size on stiffness are neglected, the laminate E_u based on units of force per unit width of specimen would be expected to be the same as Nhc_2 from the VCA tests. In Fig. 2, the VCA data are from a single specimen among the 205 g/m² papers in the MD (Table 2) but have been scaled in proportion to the average fitted curve to represent typical experimental noise.

TABLE 3—*Experimental extensional stiffness of laminates compared with summation of initial compression stiffness of paper laminations.*

		Extensional Stiffness					
		Machine Direction (MD)			Cross Machine Direction (CD)		
BW g/m²	Lam. (N)	E_u kN/m	Nhc_2[a] kN/m	Difference %	E_u kN/m	Nhc_2 kN/m	Difference %
205	1	…	1.69	…	…	0.768	…
	4	6.99	6.75	−3.44	3.16	3.07	−2.65
	5	9.16	8.43	−7.94	3.80	3.84	1.06
	6	11.5	10.1	−11.8	4.98	4.61	−7.41
244	1	…	3.02	…	…	0.502	…
	3	10.7	9.07	−15.3	1.58	1.51	−4.76
	4	12.6	12.1	−4.37	2.12	2.01	−5.28
	5	17.5	15.1	−13.8	2.99	2.51	−16.1
	6	20.7	18.1	−12.4	3.17	3.01	−5.08
342	1	…	3.95	…	…	0.765	…
	3	12.2	11.8	−2.70	2.47	2.29	−7.25
	4	16.7	15.8	−5.30	3.45	3.06	−11.3
	5	20.5	19.7	−3.80	3.98	3.82	−3.98
Average		…	…	−8.09	…	…	−6.28

[a]Characterizations of h and c_2 are given in Table 2.

With units of c_2 given in terms of stress, the initial slope of the fitted one-ply load-strain curve (Fig. 2) is given by hc_2 = 1.69 kN/m (Table 3). The predicted initial slope of the four-ply compression curve (Fig. 2) is then Nhc_2 = 6.75 kN/m. For comparison, the average E_u of actual corresponding four-ply laminates is E_u = 6.99 kN/m (Table 3). On average, predictions of Nhc_2 are 8.09 % less in the MD and 6.28 % less in the CD than are corresponding experimental E_u (Table 3). This comparison provides one measure of the predictability of packaging form performance from paper properties.

Column Compression Strength

Column compression tests were performed on all design combinations described in Table 1. Tube specimens were cut to a 305-mm

TABLE 2—*Material properties of component paper.*[a]

		Machine Direction (MD)				Cross Machine Direction (CD)				c_2CD/c_2MD Ratio
		VCA Stress–Strain Parameters		Maximum Stress (σ_u)		VCA Stress–Strain Parameters		Maximum stress (σ_u)		
BW g/m²	Thickness (h) mm	c_1 MPa	c_2 GPa	VCA MPa	Ring Crush MPa	c_1 MPa	c_2 GPa	VCA MPa	Ring Crush MPa	A
205	0.262	27.1	6.45	19.8	10.6	15.1	2.94	12.5	8.12	0.455
244	0.368	33.4	8.21	26.3	13.1	8.93	1.36	8.75	7.21	0.166
342	0.462	29.9	8.54	22.7	15.8	10.2	1.65	9.62	8.78	0.194

[a]VCA is vacuum compression apparatus.

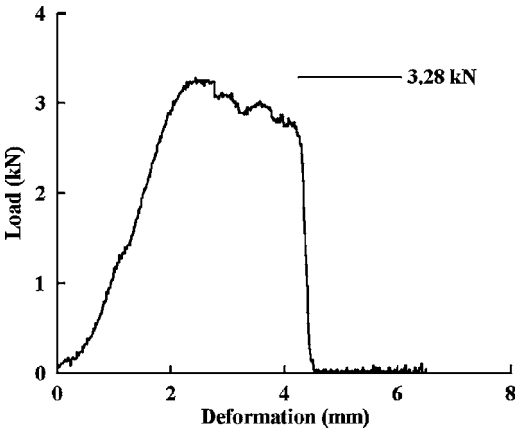

FIG. 3—*Representative load-deformation curve with 3.28-kN strength from column compression test of tubular packaging form style 155 with four laminations of 205 g/m^2 paper.*

length on a table saw equipped with a right angle guide. Compression tests in a screw-driven machine used a ball-and-socket base to ensure uniform compression around the tube perimeter. Specimen length was selected such that the machine loading speed applied to the specimen length would yield a material strain rate equal to the strain rate of VCA compression tests. Figure 3 shows a representative load-deformation curve from which the maximum load was of interest. Ten tests of each tube design were made.

Figure 4 shows a typical local buckling pattern along a tube surface in which the amplitude of the buckled wave was observed to increase as axial compression increased. The onset of the buckled wave corresponds to the critical stress σ_{cr}. As compression continues beyond the buckling load, a postbuckling[4] action redistributes the loads of buckled segments to non-buckled segments. Flat and arched segments increasingly fail by material crushing until axial loading ceases to increase and the tube strength is attained. Data on average tube strength P and the coefficient of variation (CV) are given in Table 1.

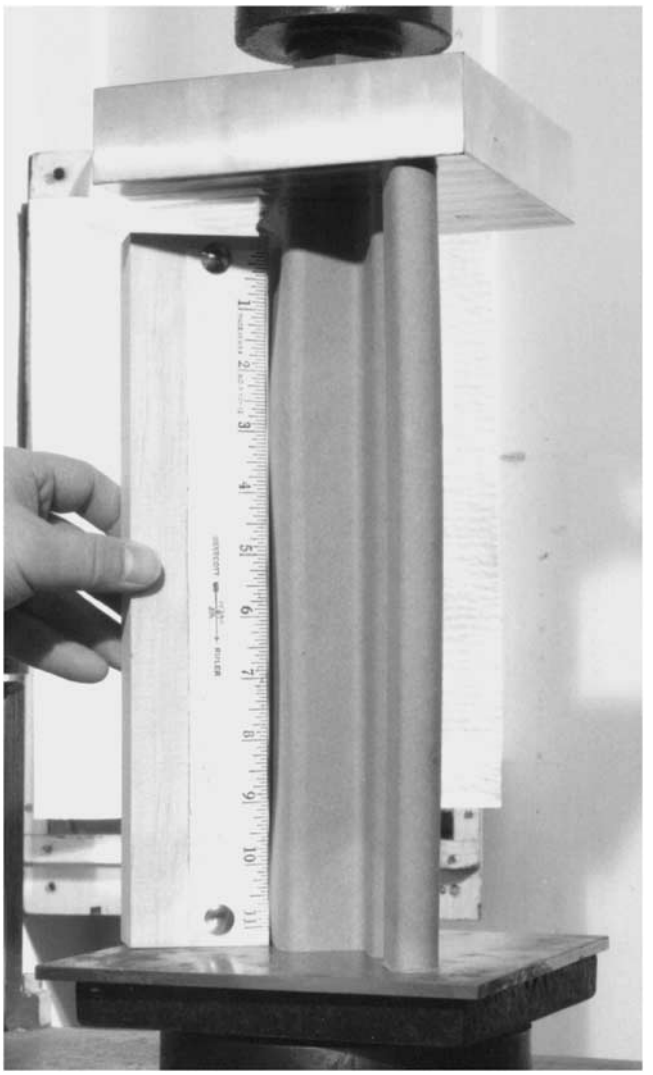

FIG. 4—*Local buckling pattern along surface of tubular packaging form subjected to column compression. Scale is in units of inches.*

Model

Each tube style (Fig. 1) is seen to be a connection of geometrically flat and arched segments. The width of a flat segment bounded between adjacent arched segments is defined to be the contiguously flat portion, as shown in Fig. 5. It was generally observed in column compression tests that tube strength is limited by the widest of the flat segments in which buckling first occurred. The total perimeter p of the tube is

$$p = \sum l + l_c \tag{2}$$

where l is the width of a flat segment sufficiently wide to buckle and l_c is a width dimension equal to the cumulative arc length of remaining flat and arched segments. The width dimensions of the flat segments determined to be wide enough to buckle are indicated in Fig. 1 for the weakest combination of BW and N. These l dimensions are also listed in Table 1. For the particular experimental design of this study, buckling prone segments for tube styles 155, 192, and 263 depend on BW and N (Table 1). In the unbuckled material represented by cumulative width dimension l_c, segments were observed to crush as column compression increased beyond the level corresponding to tube strength (Fig. 3).

To determine which segments are apt to buckle, the calculated critical stress σ_{cr} of each flat segment, in accordance with Johnson and Urbanik [2], was compared with σ_u; if $\sigma_{cr} < \sigma_u$, the segment l was counted among the buckling segments. To determine σ_{cr}, a flat plate segment was characterized by its material stress-strain law given by Eq 1 and a dimensionless segment stiffness S given by

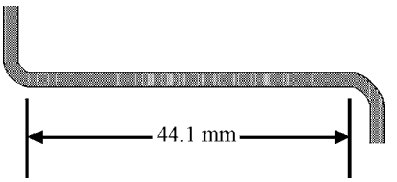

FIG. 5—*Example of flat segment from tube style 192 (Fig. 1) showing determination of 44.1-mm width from contiguously flat portion between adjacent arched segments.*

[4]As used here, postbuckling designates a mechanical phenomenon subsequent to buckling of a structure and should not be confused with buckling of a "post."

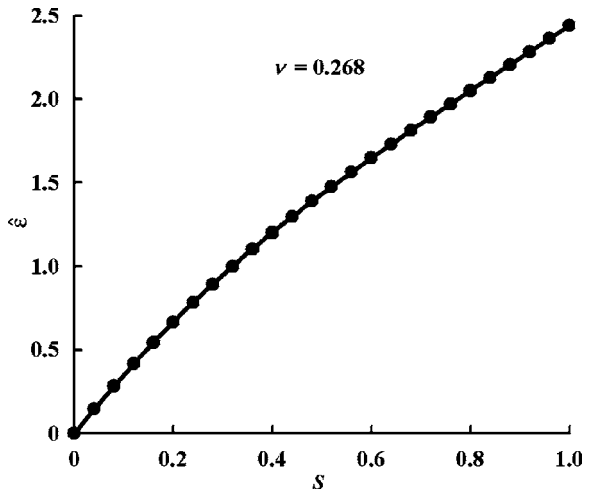

FIG. 6—*Solution of Eq 4* (*points*) *compared with approximation by Eq 5* (*line*) *for ν=0.268.*

$$S = \frac{c_2}{c_1}\left(\frac{Nh}{l}\right)^2 A^{1/2} \tag{3}$$

A normalized critical strain $\hat{\varepsilon}$ is obtained numerically solving the equation

$$\hat{\varepsilon} = \frac{\pi^2 S}{6(1-\nu^2)}\left\{1+\left[1-(1-\nu^2)\left(1-\frac{2\hat{\varepsilon}}{\sinh(2\hat{\varepsilon})}\right)\right]^{1/2}\right\} \tag{4}$$

In this formula, ν is a geometric mean Poisson's ratio. The average $\nu_1=0.268$ considered in the calculations of Johnson and Urbanik [8] was assumed to apply. The critical stress is then $\sigma_{cr}=c_1\tanh\hat{\varepsilon}$.

The complete derivation of Eqs 3 and 4 characterizing buckling of an infinitely long, simply supported plate subjected to axial compression is given by Johnson and Urbanik [2]. Although Eq 4 must be solved numerically, an accurate approximation is shown in Fig. 6 for the case $\nu=0.268$ and is given by

$$\hat{\varepsilon} = 3.712S - 2.124S^2 + 0.8527S^3 \tag{5}$$

Our experimental design resulted in one to five segments per perimeter that were apt to buckle, depending on paper basis weight and laminations, and are characterized by their respective *l*-dimension in Table 1. Universal slenderness $U=\sqrt{\sigma_u/\sigma_{cr}}$ is a criterion commonly used to differentiate between buckling and crushing modes of failure. Given the differentiation among segments according to *U*, our model for column compression strength of the tube applied the following postbuckling formula to predict the failure stress σ_f of each segment:

$$\frac{\sigma_f}{\sigma_u} = \alpha_b\left(\frac{\sigma_{cr}}{\sigma_u}\right)^{\eta} \quad U>1 \tag{6a}$$

$$\frac{\sigma_f}{\sigma_u} = \alpha_c \quad U\le 1 \tag{6b}$$

Equation 6 with empirical constants $\alpha_b=\alpha_c$ was successfully applied to the postbuckling of corrugated fiberboard panels by Urbanik [9], to fiberboard microplates by Urbanik [10], and to other paper plate elements by Urbanik and Saliklis [11]. The condition $\alpha_b=\alpha_c$ expresses the fact that as segment *S* increases, σ_{cr} approaches σ_u, *U* approaches 1, and Eq 6a approaches Eq 6b. However, as will be discussed in Results, we found it necessary to consider the form of Eq 6 with $\alpha_b\neq\alpha_c$.

TABLE 4—*Evaluation of Eq 7 parameters according to two forms.*

	Form 1		Form 2		
Tube Style	$\alpha_c=\alpha_b$	η	α_c	α_b	η
146	0.590	0.793	1.220[a]	1.220	1.855
155, 192, 363	0.590	0.793	0.490[b]	1.220	1.855
Normalized sum of errors squared	1			0.481	
Avg. prediction error magnitude, %	12.8			9.72	
r^2	0.882			0.939	

[a]For tube styles with exclusively convex curvature.
[b]For tube styles with both convex and concave curvature.

Equation 6 can be written in terms of a segment failure load P_f instead of stress to obtain

$$P_f = Nh\alpha_b\sigma_u^{1-\eta}\sigma_{cr}^{\eta} l \quad U>1 \tag{7a}$$

$$P_f = Nh\alpha_c\sigma_u l_c \quad U\le 1 \tag{7b}$$

Column compression strength is then the sum $P=\Sigma P_f$. It is helpful to also consider an apparent experimental segment stress at the experimentally determined *P*:

$$\sigma_f = \frac{P}{hl}\frac{P_f}{\sum P_f} \quad U>1 \tag{8a}$$

$$\sigma_f = \frac{P}{hl_c}\frac{P_f}{\sum P_f} \quad U\le 1 \tag{8b}$$

Results

Anecdotal reports were received of practitioners estimating tube strength with the cumulative ring crush strength. The validity of this practice was tested first by letting $\alpha_b=\alpha_c=1$ and $\eta=0$ in Eq 7 and then inputting the appropriate data (MD ring crush σ_u, Table 2). The average magnitude of the *P* prediction error was found to be 45 %, and this approach was not considered further.

Various scenarios with α_b, α_c, and η in Eq 7 empirically adjusted for geometry to obtain the best fit to data were tested next. Letting $\alpha_b=\alpha_c=0.590$ and $\eta=0.793$ for all tube styles yielded a best fitting characterization independent of geometry but with an average magnitude of prediction error of 12.8 % (form 1, Table 4). Better results were obtained by making α_b, α_c, and η dependent on tube style. Form 2 in Table 4 gives a characterization in which buckling via Eq 7a with $\alpha_b=1.220$ and $\eta=1.855$ is modeled as being the same for each tube style, but compression of tube styles 155, 192, and 263 via Eq 7b with $\alpha_c=0.490$ is modeled as being different from tube style 146 with $\alpha_c=1.220$. The average error magnitude was reduced to 9.72 %. Compared with our ability to predict E_u from paper properties, predictions of *P* from paper properties are reasonable.

Forms 1 and 2 were fit to data while minimizing the errors squared to predict *P* (Fig. 7). Alternatively, the predicted variation of σ_f/σ_u with *U* can be fitted (Fig. 8). Form 2 with three independent parameters is statistically significantly better than form 1 with two independent parameters based on the statistical F-test at the 95 % confidence level.

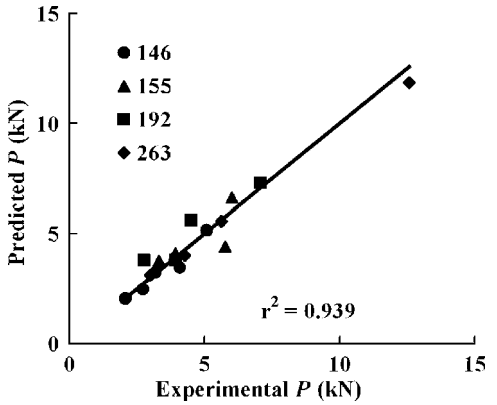

FIG. 7—*Comparison between tube strength by Eq 7 with parameter evaluations of form 2, Table 4, and data for four tube styles shown in Fig. 1. Line shows equality.*

The form of Eq 7 with σ_{cr} computed from the liner stress-strain law $\sigma = c_2\epsilon$ instead of from Eq 1 was also examined. A characterization independent of tube geometry yielded an average magnitude of prediction error of 13 % compared with 12.8 % by form 1 (Table 4). However, making α_b, α_c, and η dependent on tube style did not significantly improve the fit and it appears that a linear material law is insensitive to tube geometry.

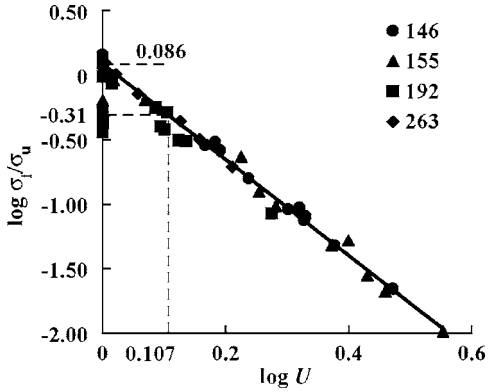

FIG. 8—*Comparison of ratio of apparent stress at failure to ultimate stress varying with universal slenderness among flat and arched segments comprising packaging form geometry shown in Fig. 1. Apparent failure stress is determined following example in Table 5. Solid line is a fit of the model given by form 2 to points corresponding to buckling failure. Points clustered around ordinate value of −0.31 correspond to compression failure. Dashed lines correspond to model parameters* (*see text*).

The characterization of tube style 146 with $\alpha_b = \alpha_c$ is consistent with the postbuckling behavior of corrugated fiberboard. Tube style 146 is unique in that all curvature is fabricated convexly to the tube perimeter (Fig. 1). In contrast, tube styles 155, 192, and 263 are fabricated with both convex and concave curvature (Fig. 1). The lower α_c value (0.490) for tube styles having concave curvature compared with the value for exclusively convex curvature ($\alpha_c = 1.220$) appears to account for a strength loss arising from fabrication-induced weakening of these laminates. However, corroborating strength tests on laminates were not conducted and this hypothesis cannot be explored further.

Example

The calculation of P is best illustrated by example. Consider tube style 192 (Fig. 1) made with three laminations of 342 g/m^2 paper. The tube perimeter is 300 mm (Table 1). The evaluations of σ_{cr} for flat segments with width $l = 44.1$, 29.6, 27.7, and 27.1 mm first need to made and compared with $\sigma_u = 22.7$ MPa (Table 2). Table 5 gives the results of calculations of S, $\hat{\epsilon}$, σ_{cr} and U for the 44.1, 29.6, and 27.7 mm segments. The 27.1 mm segment yields $\sigma_{cr} = 23.1$ MPa $> \sigma_u$. Therefore with three laminations of 342 g/m^2 paper, this segment is not counted among those that buckle and is instead analyzed as a compression segment. The width of a default compression segment is determined from the initial $l_c = p - \Sigma l$, and the value of $U = 1$ is assigned to represent the collective compression segments (Table 5).

Values of α_b, α_c, and η taken from the model given by form 2 of Table 4 are assigned to the segments based on their predicted failure mode and each P_f is determined (Table 5). Because tube style 192 includes concave curvature, the value $\alpha_c = 0.490$ is assigned. The summation predicts a strength of $\Sigma P_f = 5.63$ kN. Given ΣP_f the stress ratio σ_f/σ_u can then be computed. A plot of the experimental σ_f/σ_u varying with U for the data in Table 5 is shown in Fig. 8 along with the other tube style and paper combinations. Figure 8 provides a way to corroborate the expected postbuckling response of individual tube segments.

The calculations shown in Table 5 are easily incorporated within spreadsheet software to determine the effect of different paper properties, laminations, and l-dimensions on strength. Table 6 shows the strength predictions for tube styles 146, 155, 192, and 263 made with all combinations of BW and N considered in this study.

Certain extrapolations outside our experimental design are noteworthy. For instance, if the number of laminations is increased from four to five for tube style 155 with 205 g/m^2 paper, strength is predicted to decrease from 3.77 to 3.76 kN (Table 6). For tube style

TABLE 5—*Example analysis of tubular packaging form style 192* (*Fig. 1*) *made with three laminations of 342 g/m^2 paper.*[a]

l, Fig. 1 mm	l_c mm	S Eq 3	$\hat{\epsilon}$ Eq 5	σ_{cr} (MPa) $c_1\tanh\hat{\epsilon}$	$\frac{U}{\sqrt{\sigma_u/\sigma_{cr}}}$	Table 4			P_f (N)		σ_f/σ_u Eq 8
						α_b	α_c	η	Eq 7	Exp	
44.1	…	0.124	0.431	12.1	1.367	1.220	…	1.855	530	426	0.307
29.6	…	0.276	0.881	21.1	1.036	1.220	…	1.855	995	800	0.860
27.7	…	0.315	0.986	22.6	1.002	1.220	…	1.855	1,054	847	0.973
…	27.1	…	…	…	1	…	0.490	0	417	335	0.394
…	171	…	…	…	1	…	0.490	0	2,632	2,116	0.394
								Σ=	5,629	4,525	

[a]Paper properties and VCA determinations of c_1, c_2 and σ_u in MD shown in Table 2.

TABLE 6—*Predictions of column compression strength along with strength normalized with respect to linear mass of paper for all tube styles and test paper combinations.*

		Predicted P (kN) for Various Tube Styles				Normalized Predicted P (Nm/g) for Various Tube Styles			
BW g/m^2	Lam. (N)	146	155	192	263	146	155	192	263
205	3	0.69	2.07	1.91	1.75	4	11	10	10
205	4	1.05	3.77	3.55	3.12	4	15	14	13
205	5	1.60	3.76	3.81	4.01	5	12	12	13
205	6	2.48	4.97	5.01	5.64	7	13	14	15
244	3	1.31	4.10	3.79	3.45	6	19	17	16
244	4	2.05	6.63	7.01	6.22	7	23	24	21
244	5	3.25	7.23	7.30	7.85	9	20	20	21
244	6	5.16	9.67	9.59	11.1	12	22	22	25
342	3	1.78	4.42	5.63	5.57	5	13	17	16
342	4	3.46	6.78	6.80	7.70	8	15	15	17
342	5	6.55	10.1	7.68	11.9	12	18	14	21
342	6	11.3	14.5	9.22	10.2	17	21	14	15

263 with 342 g/m^2 paper, if the number of laminations is increased from five to six, predicted strength decreases from 11.9 to 10.2 kN (Table 6). Our model predicts that for these two cases the added paper strength is offset by a suspected fabrication-induced weakening of compression segments.

Experimental evidence of such a weakening appears in Fig. 8, specifically in the clustering of points around $U=1$ ($\log U=0$). The lower cluster of points at $\sigma_f/\sigma_u=\alpha_c=0.490(\log \sigma_f/\sigma_u=-0.31)$ characterizes tube segments that fail by compression. The upper cluster of points on the line fitted through $\sigma_f/\sigma_u=\alpha_b=1.220(\log \sigma_f/\sigma_u=0.086)$ characterizes flat segments that fail by buckling. Figure 8 and Eq 6 predict that the most efficient segments are those that fail by buckling close to the compression strength and are characterized by $0.61\sigma_u<\sigma_{cr}<\sigma_u$ ($0<\log U<0.107$).

Table 6 also shows strength predictions normalized with respect to the cumulative paper density and tube perimeter. Normalized P is a measure of efficient use of paper among the various tube designs considered. By following the procedures in these examples, new or altered tube geometries can be analyzed by reducing the geometry to a set of l and l_c dimensions.

Conclusions

Tubular packaging forms made from rolled laminations of paper, loaded along the tube axis, and used as corner posts can be considered as a sequence of segments apt to fail by either buckling or compression. The failure mode of a segment depends on the width of its contiguously flat portion along with constituent paper properties and number of laminations. The strength contribution of narrow compression segments is the summation of constituent paper strength reduced to account for fabrication-induced curvature. The strength contribution of wider buckling segments can be determined from a simplified formula derived from buckling theory appropriate for nonlinear material that accounts for material stiffness. Our model quantifies the efficiency between buckling and compression performance. Column compression strength can be predicted with an average error magnitude of 9.7 % using paper properties that predict laminate stiffness with a comparable error of 8 %. Example calculations are provided to incorporate our model within spreadsheet software. The principles of our derived model of column compression strength provide insight into the optimum paper properties and number of laminations in the selection and design of tubular posts.

References

[1] U.S. Department of Commerce, "Major Household Appliances: 2003," Current Industrial Reports, December, 2004.

[2] Johnson, M. W., Jr. and Urbanik, T. J., "Buckling of Axially Loaded, Long Rectangular Plates," *Wood Fiber Sci.*, Vol. 19, No. 2, 1987, pp. 135–146.

[3] ASTM Standard D 685-93, "Standard Practice for Conditioning Paper and Paper Products for Testing," *Annual Book of Standard*ASTM International, West Conshohocken, PA, 2002.

[4] Gunderson, D., "Edgewise Compression of Paperboard: A New Concept of Lateral Support," *Appita*, Vol. 37, No. 2, 1983, pp. 137–141.

[5] Urbanik, T. J., "Method Analyzes Analogue Plots of Paperboard Stress-Strain Data," *Tappi J.*, Vol. 65, No. 4, 1982, pp. 104–108.

[6] TAPPI Official Test Method T 411, "*Thickness* (*Caliper*) *of Paper, Paperboard, and Combined Board*," TAPPI, Atlanta, GA, 2005.

[7] TAPPI Classical Test Method T 818, "*Ring Crush of Paperboard*," TAPPI, Atlanta, GA, 1997.

[8] Johnson, M. W., Jr. and Urbanik, T. J., "A Nonlinear Theory for Elastic Plates With Application to Characterizing Paper Properties," *J. Appl. Mech.*, Vol. 51, No. 3, 1984, pp. 146–152.

[9] Urbanik, T. J., "Review of Buckling Mode and Geometry Effects on Postbuckling Strength of Corrugated Containers," *PVP, Development, Validation, and Application of Inelastic Methods for Structural Analysis and Design*, ASME, Vol. 343, 1996, pp. 85–94.

[10] Urbanik, T. J., "Correcting for Instrumentation with Corrugated Fiberboard Edgewise Crush Test Theory," *Tappi J.*, Vol. 24, No. 4, 1990, pp. 263–268.

[11] Urbanik, T. J. and Saliklis, E. P., "Finite Element Corroboration of Buckling Phenomena Observed in Corrugated Boxes," *Wood Fiber Sci.*, Vol. 35, No. 3, 2003, pp. 322–333.